STOKES-BRINKMAN LAGRANGE MULTIPLIER/FICTITIOUS DOMAIN METHOD FOR FLOWS IN PEBBLE BED GEOMETRIES

AZIZ TAKHIROV *

Abstract. This work developes an approach for numerical simulation of fluid flow through a domain with a complex geometry. We consider a finite element discretization of Stokes-Brinkman equation for modelling the incompressible viscous flow inside a fluid-solid systems combined with Lagrange multiplier/fictitious domain and special spherical bubble functions. Well-posedness of the new method, á priori estimates, and convergence results are established. Results of numerical experiments are presented and compared to the other methods.

Key Words: Navier-Stokes, Brinkman, viscous flow, porous media flow, fictitious domain.

Mathematics Subject Classification: 76D07, 76S99, 65M85.

1. Introduction. This paper presents a method for the simulation of viscous incompressible flow through pebble bed geometries. These type of flows are intermediate between free flows and porous media flows, and they occur in many important applications. While our long term goal is to simulate turbulent flows in such domains, we begin by considering the Stokes flow with few a spherical inclusions, since the geometric complexity already occurs there.

Generally slow, viscous flow inside fluid-solid system would be described by Stokes equations in the pores with no-slip boundary conditions at solid interfaces. The finite element methods based on these equations use body-fitted meshes. When the number of solid bodies is large, meshing such region becomes impractical (e.g. pebble-bed reactors contain nearly 400,000 graphite covered uranium spheres [16]).

One alternative approach is Darcy based models. But they are inadequate since

a) the Darcy models are appropriate for the flow with [2], [17] $Re_{porous} := \frac{qd}{\nu} \leq 1$, where d is the diameter of pore, ν is the kinematic viscosity and q is the specific discharge. Since the diameters of the pores are too big and velocity can be too large, the Darcy model can be inaccurate model.

b) Darcy models fail to predict recirculation regions (where the heat concentrates). Since $\mathbf{u} = -K\nabla p$, $\nabla \times \mathbf{u} = 0$.

Another approach with some promise is the Brinkman model [1], [13], [5] used as volume penalization of the flow in the solid bodies. In this method the original domain is embedded inside a geometrically simple fictitious auxiliary domain, in which flow obeys the Stokes-Brinkman equations. The particular medium is then taken into account by its characteristic permeability and viscosity, i.e. infinite permeability in the fluid region, nearly zero permeability in the solid region and very large viscosity in the solid region. That is, for a fixed small penalty parameter $\varepsilon > 0$, the Brinkman parameters are

$$\tilde{\nu} = \begin{cases} \nu & \text{if } x \text{ in Fluid region,} \\ \frac{1}{\varepsilon} + \nu & \text{if } x \text{ in Solid region} \end{cases}$$

and

$$K = \varepsilon \text{ if } x \text{ in Solid region.}$$

The Stokes-Brinkman equations are given by the following system

$$-\nabla \cdot (\tilde{\nu}\nabla \mathbf{u}) + \frac{1}{K}\mathbf{u} + \nabla p = \mathbf{f} \text{ in Solid} \cup \text{Fluid region} \tag{1.1}$$

$$\nabla \cdot \mathbf{u} = 0 \text{ in Solid} \cup \text{Fluid region} \tag{1.2}$$

*Department of Mathematics, University of Pittsburgh, Pittsburgh, PA, 15260, USA. email: azt7@pitt.edu. Partially supported by the NSF under grants DMS-0810385, DMS-1216465

where $\mathbf{f}$ is the body force, K is the permeability of the medium and $\tilde{\nu}$ is the Brinkman viscosity.

Finite element methods for the flow in the pebble beds based on the Brinkman model were investigated in [12] concluding that, *if the finite element mesh does not resolve fluid solid interface, Brinkman simulations can fail to predict reliably flow start up, heat transfer and recirculation regions.*

We show herein that for the Stokes-Brinkman problem by *imposing the no-flow condition in the solid bodies weakly through Lagrange multipliers and enhancing the velocity space by spherical bubble functions more accurate numerical results can be obtained.* Moreover, when our proposed algorithm is used, *i*) the method is more accurate compared to the Stokes-Brinkman Volume Penalization, *ii*) the convergence rate of the velocity is decoupled from the Lagrange mupltiplier and *iii*) less fluid flows through the solid region, a critical test of model fidelity. Thus, we are able to obtain accurate solutions on a simple mesh with a mathematically sound model.

The outline of this paper is as follows: the remainder of this section discusses the motivating examples for the model and introduces the notation used throughout the paper. Section 2 contains preliminaries, introduces the discrete spaces, presents the numerical method. Section 3 discusses well-posedness, stability and convergence of the method. In the last section, we present the results of the numerical experiments.

1.1. Motivating applications. Flows in pebble bed geometries occur (with many additional complexities not considered herein) e.g., in pebble bed reactors [15], [16], in optimization of close turbine placement in wind farms [18], [6] and other industrial processes. For these applications, the essential flow features such as flow start up, heat transfer and recirculation regions (in which heat concentrates) must be accurately predicted by any reasonable numerical model. Additionally, any such method must be computationally affordable, a challenge since typical flows are too fast for homogenized models and resolving the pores with mesh is impractical. Currently, the flow in such regions is not well understood yet (e.g. the temperature inside the pebble bed reactors are often off the predicted values by 200 °C [14]).

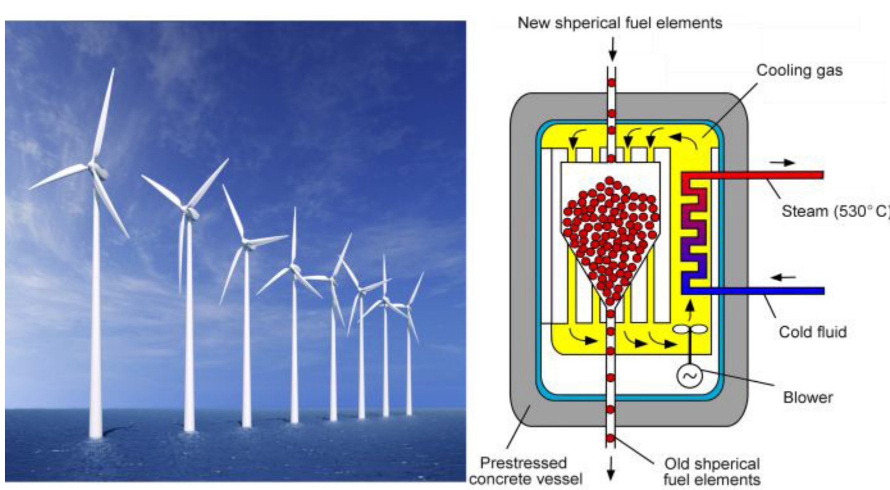

Fig. 1.1: Pebble Bed Reactor and Wind Farm

1.2. Nomenclature. We denote by Ω an open, simply connected, bounded domain in $R^d, d = 2, 3$, with Lipschitz continuous boundary. We decompose Ω into a purely fluid domain Ω_f and purely solid domain Ω_s, which is made up of disjoint union of S balls $B_i = \{\mathbf{x} \in R^d : |\mathbf{x} - \mathbf{x}_i| < r\}$ centered at $\mathbf{x}_i$ and with the same radius r. Throughout the paper we will assume that $\partial B_i \cap \partial\Omega = \emptyset,\ i = \overline{1,S}$. The characteristic function of the set ω will be denoted by χ_ω and $\mathbf{e}_i$ will denote the standard i-th basis vector of R^d. We use the notation $H^k(\Omega_*), \|\cdot\|_{k,*}, (\cdot,\cdot)_{k,*}, k \geq 0$, for the Sobolev spaces of all functions having square integrable weak derivatives up to order k on Ω_*, and the standard Sobolev norm and inner product, respectively. When $*$ is omitted, notation refers to the integral over entire Ω. When $k = 0$ we just write $L^2(\Omega_*), \|\cdot\|_*, (\cdot,\cdot)_*$ instead of $H^0(\Omega_*), \|\cdot\|_{0,*}$, and $(\cdot,\cdot)_{0,*}$, respectively. Further, $L_0^2(\Omega_*)$ will refer to the space $\{q \in L^2(\Omega_*) : \int\limits_{\Omega_*} q = 0\}$. For the seminorm in $H^k(\Omega_*)$ we use $|\cdot|_{k,*}$. $\|\cdot\|_{-1,*}$, $\|\cdot\|_{1/2,*}$ and $\|\cdot\|_{-1/2,*}$ will be used for the norms in the standard spaces $H^{-1}(\Omega_*)$, $H^{1/2}(\partial\Omega_*)$ and $H^{-1/2}(\partial\Omega_*)$. Dual space of the space Y will be denoted by Y'. Finally, $\langle\cdot,\cdot\rangle_{Y'\times Y}$ will denote the duality pairing between Y' and Y.

2. Stokes-Brinkman Lagrange Multiplier/Fictitious Domain method.

2.1. Preliminaries. We assume that $\mathbf{f} \in H^{-1}(\Omega_f)$, $\mathbf{g} \in H^{1/2}(\partial\Omega)$ and $\mathbf{g}$ satisfies the compatibility conditon

$$\int_{\partial\Omega} \mathbf{g}\cdot\mathbf{n} = 0.$$

We set $\mathbf{f} = \mathbf{0}$ in Ω_s. Next, we denote the extension of the boundary data $\mathbf{g}$ by $E\mathbf{g} \in H^1(\Omega)$, which is assumed to satisfy $E\mathbf{g} = \mathbf{0}$ in $\Omega_s, \nabla\cdot E\mathbf{g} = 0$ and $\|E\mathbf{g}\|_1 \leq C\|\mathbf{g}\|_{1/2}$. Such extension can be obtained by using smooth cut-off functions and the property of the divergence operator, as shown below.

Lemma 2.1. *[8, p. 288] Let ω be a bounded domain of R^d, $d \leq 4$ with a Lipschitz-continuous boundary Γ. For $\forall\varepsilon > 0$, there exists a function $\theta_\varepsilon \in C^2(\overline{\omega})$ such that*

$$\begin{cases} \theta_\varepsilon = 1, & \text{in a neighborhood of } \Gamma, \\ \theta_\varepsilon = 0, & \text{if } \ d(x;\Gamma) \geq 2\exp(-\frac{1}{\varepsilon}), \\ |\nabla\theta_\varepsilon| \leq C\frac{\varepsilon}{d(x;\Gamma)}, & \text{if } \ d(x;\Gamma) \leq 2\exp(-\frac{1}{\varepsilon}), \end{cases}$$

where $d(x;\Gamma) = \inf\limits_{y\in\Gamma}|x-y|$ is the distance function.

Lemma 2.2. *There exists an extension $\tilde{E}\mathbf{g} \in H^1(\Omega)$ of the boundary data $\mathbf{g} \in H^{1/2}(\partial\Omega)$ such that $\tilde{E}\mathbf{g} = \mathbf{0}$ in Ω_s and $\|\tilde{E}\mathbf{g}\|_1 \leq C\|\mathbf{g}\|_{1/2}$.*

Proof. Let E' be the right inverse of the standard trace operator $\gamma : H^1(\Omega) \to H^{1/2}(\partial\Omega)$, for which $\exists C > 0$ such that $\|E'\mathbf{g}\|_1 \leq C\|\mathbf{g}\|_{1/2}$. Set $d = \min\{d(\partial\Omega_s;\partial\Omega), 1\}$. Let $\varepsilon > 0$ be such that $d = 2 * exp(-\frac{1}{\varepsilon})$. By Lemma 2.1, there exists $\theta_\varepsilon \in C^2(\overline{\Omega})$, with $\theta_\varepsilon = 0$ in Ω_s, $\theta_\varepsilon|_{\partial\Omega} = 1$. Set $\tilde{E}\mathbf{g} = \theta_\varepsilon E'\mathbf{g}$. It easy to see that $\tilde{E}\mathbf{g}$ has the desired properties. □

Lemma 2.3. *[8, p. 24] Suppose $d \leq 3$ and $\omega \subset R^d$ is open and connected. Then, the divergence operator is an isomorphism between $V^\perp(\omega)$, where $V(\omega) = \{\mathbf{v} \in H_0^1(\omega) : \nabla\cdot\mathbf{v} = 0\}$, and $L_0^2(\omega)$. Further, $\exists\beta > 0$ such that*

$$\forall\ q \in L_0^2(\omega)\ \exists!\mathbf{v} \in V^\perp(\omega), |\mathbf{v}|_{1,\omega} \leq \frac{1}{\beta}\|q\|_\omega. \tag{2.1}$$

Definition 2.4. *Let $\mathbf{g}_h$ be an interpolant of $\mathbf{g}$ and*

$$X_* := H_0^1(\Omega_*),\ Q_* := L_0^2(\Omega_*),\ L := L^2(\Omega_s).$$

Lemma 2.5. *There exists an extension $E\mathbf{g} \in H^1(\Omega)$ of the boundary data $\mathbf{g} \in H^{1/2}(\partial\Omega)$ such that $E\mathbf{g} = \mathbf{0}$ in Ω_s, $\nabla\cdot E\mathbf{g} = 0$ and $\|E\mathbf{g}\|_1 \leq C\|\mathbf{g}\|_{1/2}$.*

Proof. Note that for $\tilde{E}\mathbf{g}$ obtained in Lemma 2.2, we have $\nabla \cdot \tilde{E}\mathbf{g} \in Q_f$, because

$$\int\limits_{\Omega_f} \nabla \cdot \tilde{E}\mathbf{g} = \int\limits_{\Omega} \nabla \cdot \tilde{E}\mathbf{g} = \int\limits_{\partial\Omega} \mathbf{g} \cdot \mathbf{n} = 0. \tag{2.2}$$

By Lemma 2.3, $\exists!$ $\mathbf{v_g} \in X_f$ such that $\nabla \cdot \mathbf{v_g} = \nabla \cdot \tilde{E}\mathbf{g}$ and $|\mathbf{v_g}|_{1,f} \leq \frac{1}{\beta}\|\nabla \cdot \tilde{E}\mathbf{g}\|_f \leq \frac{\sqrt{d}}{\beta}|\tilde{E}\mathbf{g}|_{1,f}$. Extend $\mathbf{v_g}$ by zero to Ω_s. Then $\mathbf{v_g}$ belongs to X. Let $E\mathbf{g} = \tilde{E}\mathbf{g} - \mathbf{v_g}$. Then $E\mathbf{g} = \mathbf{g}$ on $\partial\Omega$, $E\mathbf{g} = \mathbf{0}$ in Ω_s, $\nabla \cdot E\mathbf{g} = 0$ and $\|E\mathbf{g}\|_1 \leq C\|\mathbf{g}\|_{1/2}$. ☐

2.2. Weak formulations. Definition 2.6. *Let*

$$\begin{aligned}
a(\cdot,\cdot) : X \times X \to R,&\ a(\mathbf{u},\mathbf{v}) := (\tilde{\nu}\nabla\mathbf{u}, \nabla\mathbf{v}) + (K^{-1}\mathbf{u}, \mathbf{v})_s,\\
b(\cdot,\cdot) : Q \times X \to R,&\ b(q,\mathbf{v}) := -(q, \nabla \cdot \mathbf{v}),\\
c(\cdot,\cdot) : L \times X \to R,&\ c(\boldsymbol{\mu},\mathbf{v}) := (\boldsymbol{\mu}, \mathbf{v})_s,\\
l(\cdot) : X \to R,&\ l(\mathbf{v}) :=< f, \mathbf{v} >_{H^{-1}(\Omega)\times H^1(\Omega)} -\nu(\nabla E\mathbf{g}, \nabla\mathbf{v})_f,\\
l_h(\cdot) : X \to R,&\ l_h(\mathbf{v}) :=< f, \mathbf{v} >_{H^{-1}(\Omega)\times H^1(\Omega)} -\nu(\nabla E\mathbf{g}_h, \nabla\mathbf{v})_f.
\end{aligned}$$

We denote by $(\mathbf{u}, p)$ the solution of the Stokes problem in Ω_f:

$$\begin{aligned}
-\nu\Delta\mathbf{u} + \nabla p = \mathbf{f} \text{ in } \Omega_f,\\
\nabla \cdot \mathbf{u} = 0 \text{ in } \Omega_f,\\
\mathbf{u} = \mathbf{g} \text{ on } \partial\Omega,\\
\mathbf{u} = \mathbf{0} \text{ on } \partial\Omega_s,
\end{aligned} \tag{2.3}$$

prolongated by $(\mathbf{u}, p) = (\mathbf{0}, 0)$ inside Ω_s.

Now we define the weak formulation of Stokes equation. Since the discrete model is going to be defined on the entire Ω, we use the test functions $(\mathbf{v}, q) \in (X, Q)$ in all of the weak formulations.

Problem 2.7. *Find $(\tilde{\mathbf{u}}, p) \in (X_f, Q_f)$ such that $\tilde{\mathbf{u}} = \mathbf{u} - E\mathbf{g}$, $(\tilde{\mathbf{u}}, p)_{\Omega_s} = (\mathbf{0}, 0)$ and*

$$\begin{aligned}
&\nu(\nabla\tilde{\mathbf{u}}, \nabla\mathbf{v})_f - (p, \nabla \cdot \mathbf{v})_f + \langle\tau(\tilde{\mathbf{u}}, p) \cdot \mathbf{n}, \mathbf{v}\rangle\\
&=< f, \mathbf{v} >_{H^{-1}(\Omega)\times H^1(\Omega)} -\nu(\nabla E\mathbf{g}, \nabla\mathbf{v})_f + \langle\nu\nabla E\mathbf{g} \cdot \mathbf{n}, \mathbf{v}\rangle \quad \forall v \in X, \qquad (2.4)\\
&(q, \nabla \cdot \tilde{\mathbf{u}})_f = 0 \quad \forall q \in Q. \qquad (2.5)
\end{aligned}$$

where $\tau(\tilde{\mathbf{u}}, p) \cdot \mathbf{n} := p\mathbf{n} - \nu\nabla\tilde{\mathbf{u}} \cdot \mathbf{n}$ is a pseudo-traction on $\partial\Omega_s$ and $\langle\cdot,\cdot\rangle$ is duality pairing between $H^{-1/2}(\partial\Omega_s) \times H^{1/2}(\partial\Omega_s)$. In this study we assume that $\tau(\tilde{\mathbf{u}}, p) \cdot \mathbf{n} \in H^{-1/2}(\partial\Omega_s)$.

Note that, since $\tilde{\mathbf{u}} \in X_f$ and $\tilde{\mathbf{u}} = \mathbf{0}$ in Ω_s, we have that $\tilde{\mathbf{u}} \in X$. Further, as $p|_{\Omega_s} = 0$, we also have $p \in Q$. These observations allow us to rewrite (2.4)-(2.5) in terms of linear operators and bilinear forms defined in Definition 2.6.

Problem 2.8. *Find $(\tilde{\mathbf{u}}, p) \in (X, Q)$ such that $\tilde{\mathbf{u}} = \mathbf{u} - E\mathbf{g}$, $(\tilde{\mathbf{u}}, p)_{\Omega_s} = (\mathbf{0}, 0)$ and*

$$a(\tilde{\mathbf{u}}, \mathbf{v}) + b(p, \mathbf{v}) + \langle\tau(\tilde{\mathbf{u}}, p) \cdot \mathbf{n}, \mathbf{v}\rangle = l(\mathbf{v}) + \langle\nu\nabla E\mathbf{g} \cdot \mathbf{n}, \mathbf{v}\rangle \quad \forall v \in X, \tag{2.6}$$

$$b(q, \tilde{\mathbf{u}}) = 0 \quad \forall q \in Q. \tag{2.7}$$

The discrete model. We enhance the Stokes-Brinkman Volume Penalization model (1.1)-(1.2) with two new ingredients:

1. For a fixed, parameter $0 < \varepsilon << 1$, we impose $\mathbf{u} \simeq \mathbf{0}$ in the each ball weakly through a Lagrange Multiplier $\boldsymbol{\lambda} \in L^h := span\left\{\mathbf{e}_i\chi_{B_j} : \text{for } i = \overline{1,d}, j = \overline{1,S}\right\}$:

$$\int\limits_{B_i} \mathbf{u}\boldsymbol{\mu} = \varepsilon \int\limits_{B_i} \boldsymbol{\lambda}\boldsymbol{\mu}\ \forall \mu \in L^h.$$

2. In order to capture the geometry of the solid region, we augment the discrete velocity space with bubble functions described in the next subsection.

Note that, the standard fictitious domain method would require $L \subset H^1(\Omega_s)$ [9]. Our choice of L can be considered as non-conforming, which can be used to simplify the calculations.

PROBLEM 2.9. *Find* $(\tilde{\mathbf{u}}_h, p_h, \boldsymbol{\lambda}_h) \in (X_h, Q_h, L_h) \subset (X, Q, L)$ *such that* $\mathbf{u}_h = \tilde{\mathbf{u}}_h + E\mathbf{g}_h$ *and*

$$a(\tilde{\mathbf{u}}_h, \mathbf{v}_h) + b(p_h, \mathbf{v}_h) + c(\boldsymbol{\lambda}_h, \mathbf{v}_h) = l_h(\mathbf{v}_h) \quad \forall \mathbf{v}_h \in X_h, \tag{2.8}$$

$$b(q_h, \tilde{\mathbf{u}}_h) = 0 \quad \forall q_h \in Q_h, \tag{2.9}$$

$$c(\boldsymbol{\mu}_h, \tilde{\mathbf{u}}_h) = \varepsilon(\boldsymbol{\lambda}_h, \boldsymbol{\mu}_h)_s \quad \forall \boldsymbol{\mu}_h \in L_h. \tag{2.10}$$

2.3. Discrete subspaces. We denote conforming velocity, pressure finite element polynomial spaces based on an edge to edge triangulations of Ω (with maximum element diameter h) by

$$Y_h \subset X, Q_h \subset Q.$$

We assume that Y_h, Q_h satisfy the usual inf-sup stability condition [8], [4]. This means the velocity-pressure spaces Y_h, Q_h, before augmentation by spherical bubbles, would be div-stable for Stokes flow in Ω. In order to capture the geometry of the solid region, we additionally augment the velocity space with the spherical bubbles described below.

When choosing the spherical bubbles two things must be taken into account. First, each such basis function must be in X. Next, it should be able to capture the geometry the of balls. So ideally each such basis function $\boldsymbol{\xi}_{\mathbf{i}}$ must vanish outside $\overline{B_i}$.

For a ball B_i, define

$$\phi_i := \max\left\{1 - \frac{|\mathbf{x} - \mathbf{x}_i|^2}{r^2}, 0\right\}.$$

Now, for each ball B_i of radius r, centered at $\mathbf{x}_i$, we let $\boldsymbol{\xi}_i^j = \phi_i \mathbf{e}_j, j = \overline{1,d}, i = \overline{1,S}$.

Let

$$Z_h = span\{\boldsymbol{\xi}_1^1, \boldsymbol{\xi}_2^1, ..., \boldsymbol{\xi}_S^1, ..., \boldsymbol{\xi}_1^d, \boldsymbol{\xi}_2^d, ..., \boldsymbol{\xi}_S^d\}$$

and $X_h := Y_h \oplus Z_h$. Note that with this choice of bubbles, the $d * S \times d * S$ block in the stiffness matrix corresponding to Z_h will be of the form $c_1 I$, where I is the identity matrix and c_1 is a constant that can be pre-computed.

3. Well-posedness, stability and convergence. In this section, we prove well-posedness of the system (2.8)-(2.10), along with stability and convergence results.

DEFINITION 3.1. *Let* $\|\cdot\|_\varepsilon^2 := \nu|\cdot|_1^2 + \frac{1}{\varepsilon}\|\cdot\|_{1,s}^2$.

LEMMA 3.2. *The linear functionals* $l(\cdot), l_h(\cdot)$ *are continuous. In particular, for any* $\mathbf{v} \in X$, $q \in Q$

$$l(\mathbf{v}) \leq C(\|\mathbf{f}\|_{-1} + \nu\|\mathbf{g}\|_{1/2})|\mathbf{v}|_1,$$
$$l_h(\mathbf{v}) \leq C(\|\mathbf{f}\|_{-1} + \nu\|\mathbf{g}_h\|_{1/2})|\mathbf{v}|_1.$$

Proof. The results follow directly by applying Cauchy-Schwarz and Poincaré inequalities. ◻

LEMMA 3.3. *The bilinear functionals $a(\cdot,\cdot), b(\cdot,\cdot)$ and $c(\cdot,\cdot)$ are continuous. Further, $a(\cdot,\cdot)$ is coercive. In particular, for any $\mathbf{u},\mathbf{v}\in X$, $q\in Q$ and $\boldsymbol{\mu}\in L$,*

$$\begin{aligned}
a(\mathbf{v},\mathbf{v}) &= \|\mathbf{v}\|_\varepsilon^2,\\
a(\mathbf{u},\mathbf{v}) &\le \|\mathbf{u}\|_\varepsilon\|\mathbf{v}\|_\varepsilon,\\
b(q,\mathbf{v}) &\le \sqrt{d}\|q\||\mathbf{v}|_1,\\
c(\boldsymbol{\mu},\mathbf{v}) &\le C(\Omega)\|\boldsymbol{\mu}\|_s|\mathbf{v}|_1.
\end{aligned}$$

Proof. As in the last lemma, all the inequalities are directly obtained by applying Cauchy-Schwarz and Poincaré inequalities. ☐

THEOREM 3.1. *There exists a unique $(\tilde{\mathbf{u}}_h, p_h, \boldsymbol{\lambda}_h)\in(X_h,Q_h,L_h)$ satisfying Stokes-Brinkman-FD/LM, Problem 2.9. Moreover, $(\tilde{\mathbf{u}}_h, p_h, \boldsymbol{\lambda}_h)$ satisfy*

$$|\tilde{\mathbf{u}}_h|_1 \le C\left(\frac{1}{\nu}\|\mathbf{f}\|_{-1}+\|\mathbf{g}_h\|_{1/2}\right), \tag{3.1}$$

$$\|\tilde{\mathbf{u}}_h\|_\varepsilon \le C\left(\frac{1}{\sqrt{\nu}}\|\mathbf{f}\|_{-1}+\sqrt{\nu}\|\mathbf{g}_h\|_{1/2}\right), \tag{3.2}$$

$$\|\tilde{\mathbf{u}}_h\|_{1,s} \le C\left(\sqrt{\frac{\varepsilon}{\nu}}\|\mathbf{f}\|_{-1}+\sqrt{\varepsilon\nu}\|\mathbf{g}_h\|_{1/2}\right), \tag{3.3}$$

$$\|\boldsymbol{\lambda}_h\|_s \le C\left(\sqrt{\frac{1}{\varepsilon\nu}}\|\mathbf{f}\|_{-1}+\frac{1}{\sqrt{\varepsilon}}\|\mathbf{g}_h\|_{1/2}\right), \tag{3.4}$$

$$\|p_h\| \le C\left(\sqrt{\nu+\frac{1}{\varepsilon}}|\tilde{\mathbf{u}}_h|_1+\nu\|\mathbf{g}_h\|_{1/2}+\|\mathbf{f}\|_{-1}+\|\boldsymbol{\lambda}_h\|_s\right). \tag{3.5}$$

Proof. We first obtain the bounds (3.1)-(3.5). Restricting the test functions to $V_h = \{\mathbf{v}_h\in X_h : b(q_h,\mathbf{v}_h)=0\ \forall q_h\in Q_h\}$, reduces the Problem 2.9 to finding $(\tilde{\mathbf{u}}_h,\boldsymbol{\lambda}_h)\in(X_h,L_h)$ such that

$$a(\tilde{\mathbf{u}}_h,\mathbf{v}_h)+c(\boldsymbol{\lambda}_h,\mathbf{v}_h) = l_h(\mathbf{v}_h)\quad \forall \mathbf{v}_h\in V_h, \tag{3.6}$$
$$c(\boldsymbol{\mu}_h,\tilde{\mathbf{u}}_h) = \varepsilon(\boldsymbol{\lambda}_h,\boldsymbol{\mu}_h)\quad \forall \boldsymbol{\mu}_h\in L_h. \tag{3.7}$$

Setting $\mathbf{v}_h=\tilde{\mathbf{u}}_h, \boldsymbol{\mu}_h=\boldsymbol{\lambda}_h$ yields

$$\|\tilde{\mathbf{u}}_h\|_\varepsilon^2+\varepsilon\|\boldsymbol{\lambda}_h\|_s^2 = l_h(\tilde{\mathbf{u}}_h). \tag{3.8}$$

Applying the results of Lemmas 3.2, 3.3 and the definiton of $\|\cdot\|_\varepsilon$, we obtain (3.1)-(3.4). By assumption on (Y_h,Q_h) space, $\exists\beta_h>0$ and $\exists\mathbf{v}_h\in X_h$ such that

$$\|p_h\| \le \frac{C}{\beta}\sup_{\mathbf{v}_h\in X_h}\frac{|a(\tilde{\mathbf{u}}_h,\mathbf{v}_h)|+|c(\boldsymbol{\lambda}_h,\mathbf{v}_h)+|l_h(\mathbf{v}_h)|}{|\mathbf{v}_h|} \tag{3.9}$$
$$\le C\left(\sqrt{\nu+\frac{1}{\varepsilon}}|\tilde{\mathbf{u}}_h|_1+\nu\|\mathbf{g}_h\|_{1/2}+\|\mathbf{f}\|_{-1}+\|\boldsymbol{\lambda}_h\|_s\right). \tag{3.10}$$

In order to show existence and uniqueness of the solution, we set $\mathbf{f} = \mathbf{g}_h = \mathbf{0}$. Then (3.1)-(3.5) imply that $(\tilde{\mathbf{u}}_h, p_h, \boldsymbol{\lambda}_h) = (\mathbf{0}, 0, \mathbf{0})$. ∎

THEOREM 3.2. *Let $(\mathbf{u}, p)$ be the solution of Stokes Problem 2.8. Then we have*

$$\sqrt{\varepsilon}\|\boldsymbol{\lambda}_h\|_s + \|\tilde{\mathbf{u}} - \tilde{\mathbf{u}}_h\|_\varepsilon \leq \inf_{(\mathbf{w}_h, q_h)\in(V_h,Q_h)} C\left(\|\tilde{\mathbf{u}} - \mathbf{w}_h\|_\varepsilon + \frac{1}{\sqrt{\nu}}\|p - q_h\|\right)$$
$$+C\sqrt{\varepsilon}\left(\|\tau\cdot\mathbf{n}\|_{-1/2,s} + \nu\|\nabla E\mathbf{g}\cdot\mathbf{n}\|_{-1/2,s}\right) + \frac{C}{\sqrt{\nu}}\|\mathbf{g} - \mathbf{g}_h\|_{1/2}. \tag{3.11}$$

$$\inf_{\mathbf{w}_h\in V_h} |\tilde{\mathbf{u}} - \mathbf{w}_h|_1 \leq C\left(1 + \frac{1}{\beta_h}\right)\inf_{\mathbf{v}_h\in X_h} |\tilde{\mathbf{u}} - \mathbf{v}_h|_1. \tag{3.12}$$

Proof. Fix $0 < \varepsilon << 1$. Consider $\mathbf{v}_h, \mathbf{w}_h \in V_h,\ q_h \in Q_h$. By subtracting (2.8) from (2.6), then adding and subtracting $a(\mathbf{w}_h, \mathbf{v}_h)$ and using the fact that $c(\boldsymbol{\lambda}_h, \tilde{\mathbf{u}}) = 0$, we find

$$a(\tilde{\mathbf{u}}_h - \mathbf{w}_h, \mathbf{v}_h) + c(\boldsymbol{\lambda}_h, \tilde{\mathbf{u}} + \mathbf{v}_h) = a(\tilde{\mathbf{u}} - \mathbf{w}_h, \mathbf{v}_h) + b(p - q_h, \mathbf{v}_h) + \langle\tau\cdot\mathbf{n}, \mathbf{v}_h\rangle$$
$$- \nu\langle\nabla E\mathbf{g}\cdot\mathbf{n}, \mathbf{v}_h\rangle + (\nabla E(\mathbf{g} - \mathbf{g}_h), \nabla\mathbf{v}_h)_f. \tag{3.13}$$

Let us now choose $\mathbf{v}_h = \tilde{\mathbf{u}}_h - \mathbf{w}_h \in V_h$. Note that

$$c(\boldsymbol{\lambda}_h, \tilde{\mathbf{u}} + \tilde{\mathbf{u}}_h - \mathbf{w}_h) = \varepsilon\|\boldsymbol{\lambda}_h\|_s^2 + c(\boldsymbol{\lambda}_h, \tilde{\mathbf{u}} - \mathbf{w}_h).$$

Last identity together with the regularity assumption on pseudo-traction $\tau(\tilde{\mathbf{u}}, p)$, Lemma 3.3, (2.10) and standard inequalities imply

$$\sqrt{\varepsilon}\|\boldsymbol{\lambda}_h\|_s + \|\tilde{\mathbf{u}}_h - \mathbf{w}_h\|_\varepsilon \leq C\left(\|\tilde{\mathbf{u}} - \mathbf{w}_h\|_\varepsilon + \frac{1}{\sqrt{\nu}}\|p - q_h\|\right)$$
$$+ C\sqrt{\varepsilon}\left(\|\tau\cdot\mathbf{n}\|_{-1/2,s} + \nu\|\nabla E\mathbf{g}\cdot\mathbf{n}\|_{-1/2,s}\right) + \frac{C}{\sqrt{\nu}}\|\mathbf{g} - \mathbf{g}_h\|_{1/2}. \tag{3.14}$$

from which we have (3.11) by applying the triangle inequality.

Let us prove now the estimate (3.12). To this end choose $\forall\mathbf{v}_h \in X_h$ and $\forall\mathbf{w}_h \in V_h$. By equation (1.12) [7, p. 60]

$$|\mathbf{v}_h - \mathbf{w}_h|_1 \leq C\sup_{q_h\in Q_h}\frac{b(q_h, \mathbf{v}_h - \mathbf{w}_h)}{\|q_h\|} \leq C\sup_{q_h\in Q_h}\frac{b(q_h, \tilde{\mathbf{u}} - \mathbf{v}_h)}{\|q_h\|} \leq C|\tilde{\mathbf{u}} - \mathbf{v}_h|_1. \tag{3.15}$$

Hence,

$$|\tilde{\mathbf{u}} - \mathbf{w}_h|_1 \leq C\left(1 + \frac{1}{\beta_h}\right)|\tilde{\mathbf{u}} - \mathbf{v}_h|_1.$$

whence the estimate (3.12) follows. ∎

4. Numerical experiments. For our computations, we used $X_h = Y_h \oplus Z_h, Q_h$ and $L_h := span\left\{\begin{pmatrix}\chi_{B_i}\\0\end{pmatrix}, \begin{pmatrix}0\\\chi_{B_j}\end{pmatrix}\right\}$, where (Y_h, Q_h) are P3-P2 Taylor-Hood elements which are known to satisfy the inf-sup condition [3, 4]. We used FreeFEM++ [10] in our computations. Our tests here are preliminary proof of concept, tested in 2d with spheres simple enough to allow a mesh-conforming "true" solution to be obtained.

Two key comparisons of Brinkman (M1) vs. our model (M2) are the 1) amount of fluid flowing through the spheres and 2) the size of the dead zones behind the spheres caused by the spheres acting like a solid obstacles.

Flow through a thin channel. Our experiment is for two-dimensional flow around seven balls placed in the channel, with small distance apart from each other. The domain is $([0,1]\times[0.39,0.61])-\Omega_s$, where Ω_s is the union of seven balls with radii 0.03 and centered at $(0.16,0.49),(0.23,0.52),(0.28,0.43),(0.1,0.44),(0.13,0.56),(0.35,0.48)$ and $(0.39,0.54)$. We assume no-slip boundary conditions on the top and bottom boundaries, a parabolic inflow given by $((y-0.39)(0.61-y)/25,0)^T$ and do-nothing outflow. We take $\nu = 100$, $\mathbf{f} = (y,0)^T\chi_f$.

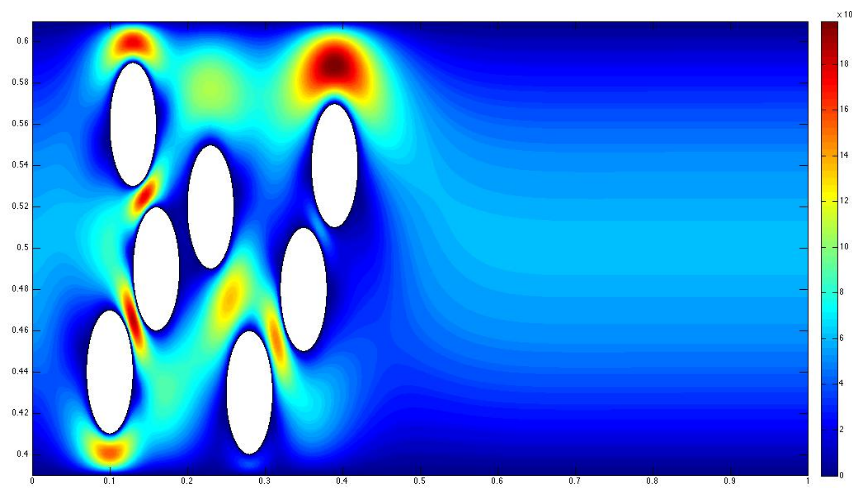

Fig. 4.1: The body-fitted, resolved Stokes speed contours

In Figure 4.1 we present the speed contour of the true solution. We ran tests on few mesh refinements (Fig. 4.2) for two different values of the penalty parameter ε.

The speed contours of our approximiations are presented in Figures 4.3-4.6, 4.8, 4.10. We also include the plots for M1 in Figures 4.7,4.9 and 4.11.

Next, we list tables of errors in Tables 4.1, 4.2.

	$\varepsilon = 1e-15$				$\varepsilon = h^2$			
	M1	rate	M2	rate	M1	rate	M2	rate
h								
0.11	3.79e-2	4.0316	2.43e-3	-0.1226	1.59e-3	0.0288	9.33e-4	0.3656
0.055	2.32e-3	0.7407	2.65e-3	0.9002	1.55e-3	0.0258	7.24e-4	0.1983
0.027	1.39e-3	0.4225	1.42e-3	0.4496	1.52e-3	0.0131	6.31e-4	1.2753
0.014	1.04e-3	-	1.04e-3	-	1.51e-3	0.001	2.6e-4	0.5746
0.007	Out of memory				1.5e-3	-	1.75e-4	-

Table 4.1: L^2 errors and rates

From the numerical experiments, we can observe the following:

- On the coarsest mesh, for both values of ε the proposed method gives much better results than M1. In the case of $\varepsilon = h^2$, M2 gives reasonable speed contours (Fig 4.3), while M1 yields very poor approximation even on the finest mesh (Fig. 4.7).

Fig. 4.2: Three coarsest meshes and Ω_s

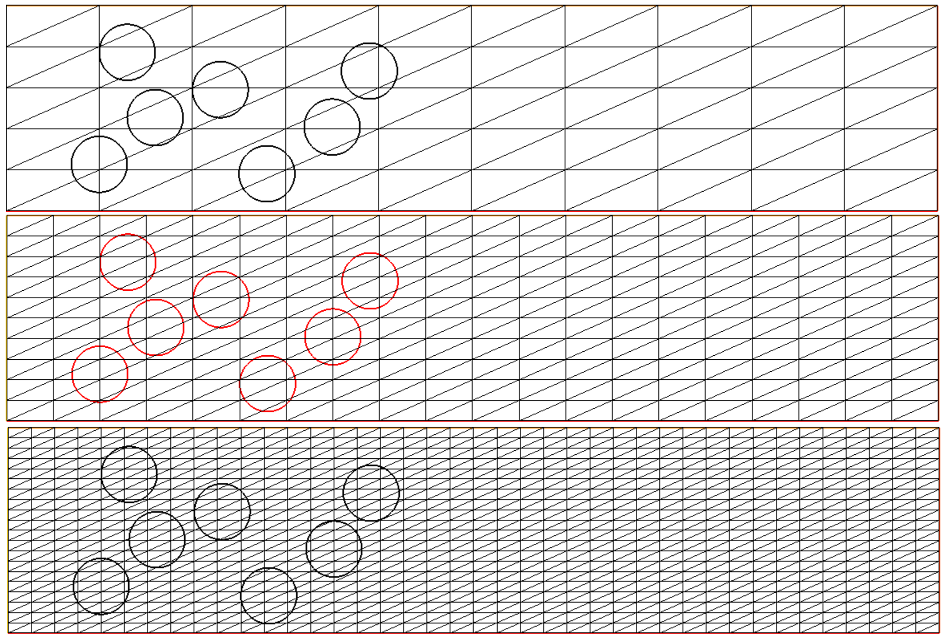

	$\varepsilon = 1e-15$				$\varepsilon = h^2$			
	M1	rate	M2	rate	M1	rate	M2	rate
h								
0.11	2.03e-3	3.99	9.145e-6	-0.782	6.9710e-4	0.022	4.548e-4	0.322
0.055	3.7607e-5	1.465	1.572e-5	2.205	6.8202e-4	0.021	3.6373e-4	0.586
0.027	8.6936e-6	2.187	2.769e-6	2.897	6.6806e-4	0.011	2.4238e-4	1.371
0.014	9.7618e-7	-	3.718e-7	-	6.6079e-4	-	9.37e-5	1.815
0.007	Out of memory				1.5e-3	-	2.6632e-5	-

Table 4.2: $L^2(\Omega_s)$ errors and rates

Further, M1 also produces more accurate approximation (Tables 4.1-4.2). This is due to the new ingredients added to Stokes-Brinkman model.

- For very small value of the penalty parameter ε, both methods give very similar, poor results. In particular note the *polygonal no-flow regions* in Figures 4.8 - 4.11. Further, the flow has been chocked off in some of the pores. One advantage of the method herein is that less flow goes through the solid domain. This improvement is due to the addition of the bubbles because, by Hólder's inequality $\int\limits_B \mathbf{u} \leq \left|\int\limits_B \mathbf{u}\right| \leq C\|\mathbf{u}\|_s \leq C\sqrt{\varepsilon}$ by (3.3), so that weak no-flow is almost satisfied for both methods.
- For larger value of ε, M2 gives very good approximiations, while M1 gives very underresolved solution even on the finest mesh.

5. Conclusions. We proposed a modification of Brinkman model for fluid flow. It avoids using computationally expensive body-fitted meshes and approximates the flow much more accurately than the original model. The analysis is valid for both 2d and 3d flows.

In this article, we have shown that the model is well-posed on any shape regular mesh. It converges at a rate $\mathcal{O}(\sqrt{\varepsilon})$ in $H^1(\Omega_s)$. Also, we proved a convergence result, where the convergence of the velocity is decoupled from that of the Lagrange multiplier.

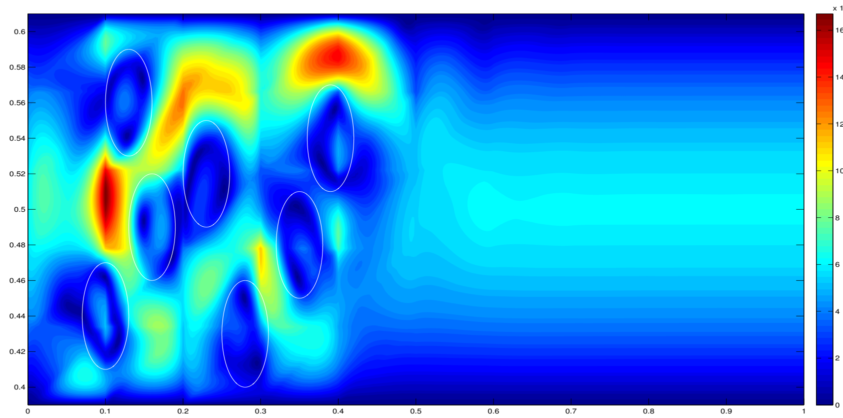

Fig. 4.3: M2, $h = 0.11, \varepsilon = h^2$

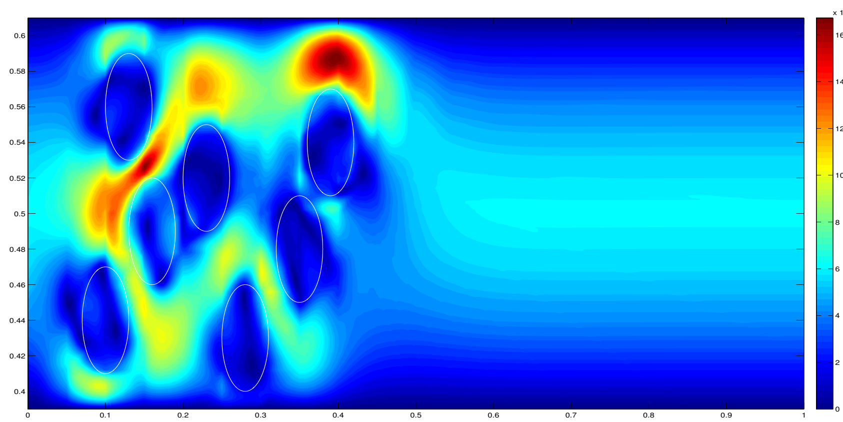

Fig. 4.4: M2, $h = 0.055, \varepsilon = h^2$

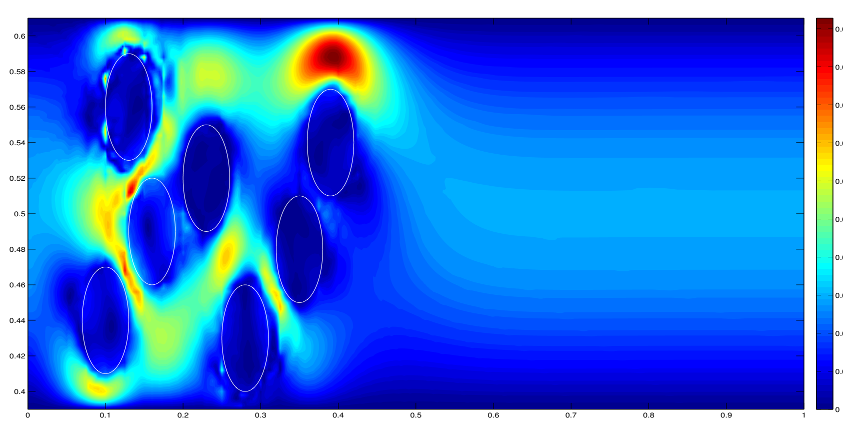

Fig. 4.5: M2, $h = 0.027, \varepsilon = h^2$

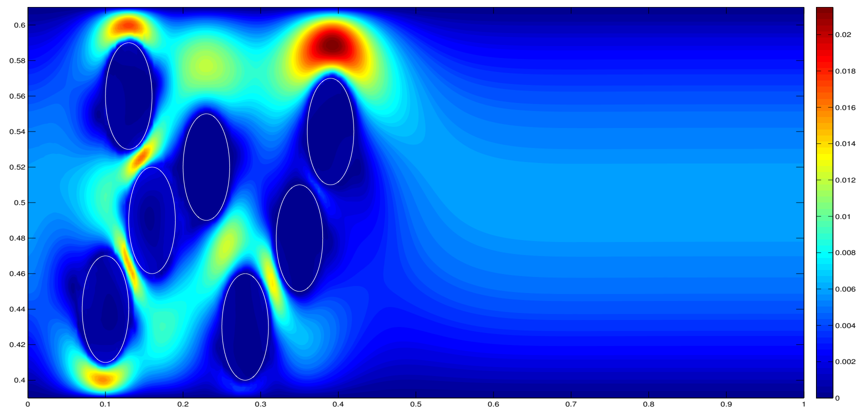

Fig. 4.6: M2, $h = 0.014, \varepsilon = h^2$

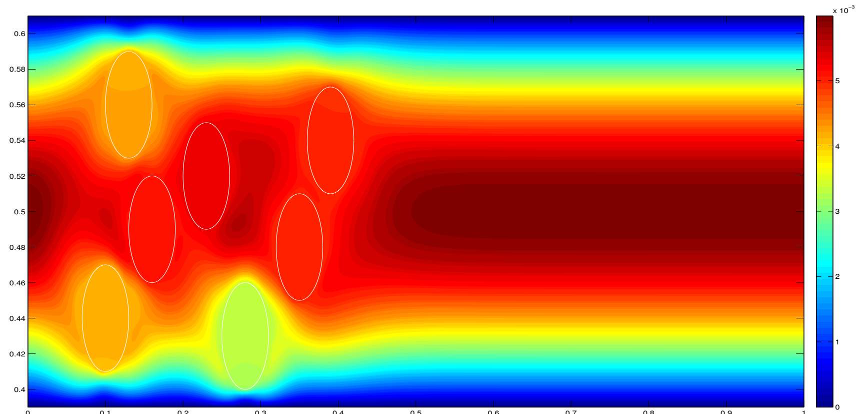

Fig. 4.7: M1, $h = 0.007, \varepsilon = h^2$

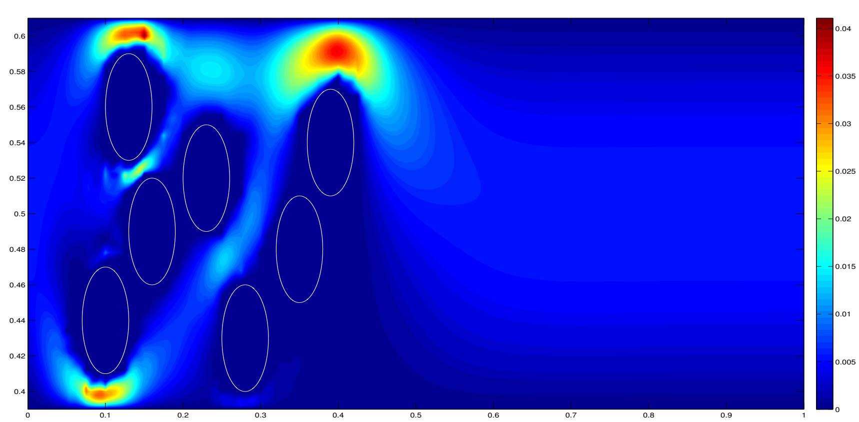

Fig. 4.8: M2, $h = 0.027, \varepsilon = 1e - 15$

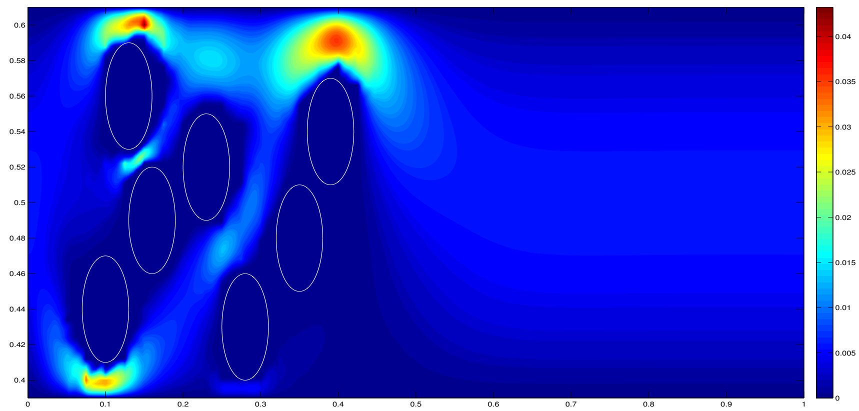

Fig. 4.9: M1, $h = 0.027, \varepsilon = 1e - 15$

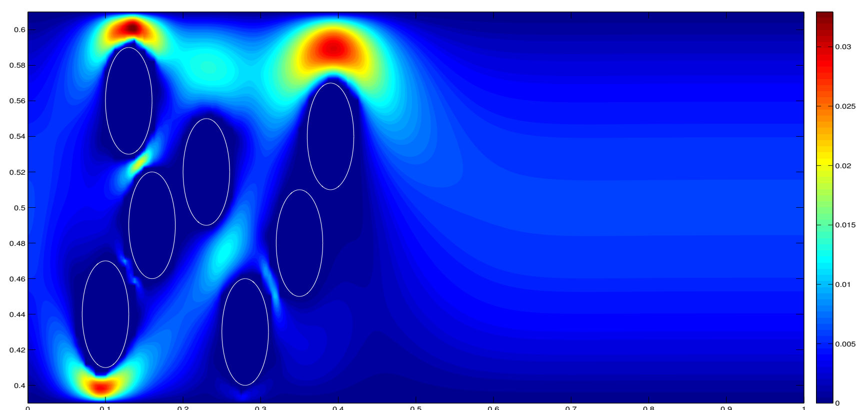

Fig. 4.10: M2, $h = 0.014, \varepsilon = 1e - 15$

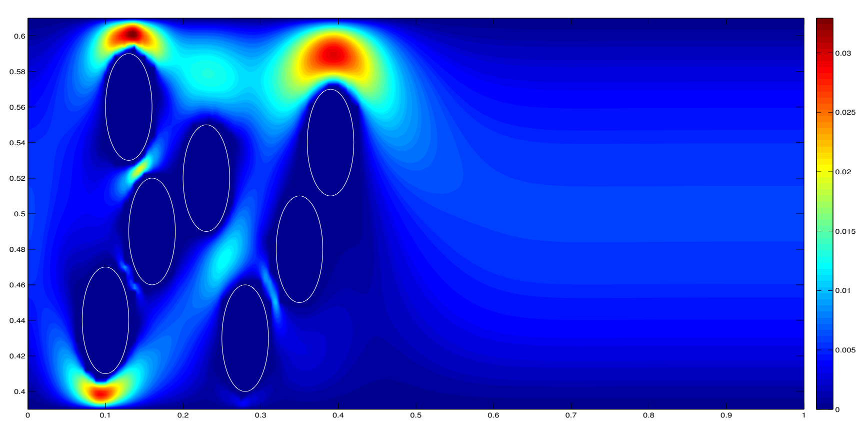

Fig. 4.11: M1, $h = 0.014, \varepsilon = 1e - 15$

The next step is the analysis and testing in the nonlinear case, followed by the coupling with heat transfer equations for high Re number flows.

Acknowledgement. Thank you, Prof. William Layton, for the brilliant ideas, discussions, and constant encouragement.

REFERENCES

[1] E. Arquis and J. P. Caltagirone, *Sur les conditions hydrodynamiques au voisinage d'une interface milieu fluide - milieu poreux: application á la convection naturellé* , C. R. Acad. Sci, Paris, Série II, 299 (1984), pp. 1-4.
[2] J. Bear, *Dynamics of fluids in porous media*, Dover, 1972.
[3] S. Brenner and L.R. Scott, *The Mathematical Theory of Finite Element Methods*, Springer-Verlag, 2008.
[4] F. Brezzi and M. Fortin, *Mixed and hybrid finite elements methods*, Springer-Verlag, 1992.
[5] H.C. Brinkman, *On the permeability of media consisting of closely packed porous particles*, Applied Scientific Research, 1(1) (1947), pp. 81-86.
[6] S.A. Grady, M.Y. Hussaini and M.M. Abdullah, *Placement of wind turbines using genetic algorithms*, Renewable energy, 30 (2005), pp. 259-270.
[7] V. Girault and P. A. Raviart, *Finite element methods for Navier-Stokes equations*, Springer-Verlag, 1979.
[8] V. Girault and P. A. Raviart, *Finite element methods for Navier-Stokes equations : theory and algorithms*, Springer-Verlag, 1986.
[9] R. Glowinski, T.W. Pan and J. Périaux, *Distributed Largange multiplier methods for incompressible viscous flow around moving rigin bodies*, in Comput. Methods Appl. Mech. Engrg. 151 (1998), pp. 181-194.
[10] F. Hecht and O. Pironneau, *FreeFEM++* , webpage: http://www.freefem.org.
[11] R. Ingram, *Finite Element Approximation of Nonsolenoidal, Viscous Flows around Porous and Solid Obstacles*, SIAM J. Numer. Anal., 49(2) (2011), pp. 491-520.
[12] R. Ingram, *Approximating fast, viscous fluid flow in complicated domains,* PhD Thesis, University of Pittsburgh (2011).
[13] K. Khadra, P. Parneix, S. Angot and J. P. Caltagirone, *Fictitous domain approach for numerical modelling of Navier-Stokes equations*, Internat. J. Numer. Methods Fluids, 34(8) (2000), pp. 651-684.
[14] R Moormann, *A safety re-evaluation of the AVR pebble bed reactor operation and its consequences for future HTR concepts*, Forschungszentrum Jlich, Zentralbibliothek, Verlag, Berichte des Forschungszentrums Jlich JUEL-4275, 2008.
[15] C.H. Rycroft, G.S. Grest, J.W. Landry and M.Z. Bazant, *Dynamics of random packings in granular flow* , Phys. Rev. E, 73(3) (2006), 051306.
[16] C.H. Rycroft, G.S. Grest, J.W. Landry and M.Z. Bazant, *Analysis of granular flow in a pebble-bed nuclear reactor*, Phys. Rev. E, 74(3) (2006), 021306.
[17] Marcelo J. S. De Lemos, *Turbulence in Porous Media: Modeling And Applications*, Elsevier, 2006.
[18] G. Marmidis, C.Y. Zhao and E. Pyrgioti, *Optimal placement of wind turbines in a wind park using monte carlo simulation*, Renewable energy, 33 (2008), pp. 1455-1460.